Spin-polarized electrons produced by strong-field ionization

Ingo Barth and Olga Smirnova
Max Born Institute, Max-Born-Str. 2A, D-12489 Berlin, Germany
(Received 18 December 2012; published 1 July 2013)

We show that ionization of noble gas atoms by a strong infrared circularly polarized laser field under standard experimental conditions can yield electrons with up to 100% spin polarization in energy-resolved measurements. Spin polarization arises due to the interplay of the electron-core entanglement and the sensitivity of ionization in circularly polarized fields to the sense of electron rotation in the initial state.

DOI: 10.1103/PhysRevA.88.013401 PACS number(s): 32.80.Rm, 42.50.Hz, 33.80.Wz

Coherent ultrashort light [1] and electron beams [1,2] produced during the interaction of atoms, molecules, and solids with strong infrared laser fields are promising new tools for ultrafast spectroscopy. Photoelectrons extracted by the strong laser field from the metal nanotip can form intense, few tens of femtosecond long coherent electron pulses [2], opening new opportunities for ultrafast electron diffraction within a table top setup. Photoelectrons produced via strong-field ionization of atoms and molecules can serve as an attosecond probe of optical tunneling [3–6], molecular structure [7,8], and dynamics [9]; their coherence can be used to record holographic images of atomic core [8,10]. We show that, when produced by ionization in a strong infrared circularly polarized field under standard experimental conditions [3–6], coherent ultrashort photoelectron pulses can have a high and controllable degree of spin polarization, opening new opportunities for attosecond spectroscopy.

Analyzing one-photon ionization, Fano [11] has shown that usually weak effects of the spin-orbit interaction are strongly enhanced in the vicinity of the Cooper minima in the photoionization continua, leading to 100% spin polarization within a certain energy window. In the one-photon ionization, spin polarization can also be achieved via ionization from a particular fine structure level of an atom or a molecule [12]. Elegant extension to resonant multiphoton ionization in the weak-field (perturbative) limit has been proposed by Lambropoulos [13–15]. Importantly, it has been demonstrated that a high degree of spin polarization is not always associated with minima in cross sections [16,17]. For example, 100% spin polarization is achieved away from the minimum in the three-photon ionization cross section of alkali-metal atoms [16], and at the maximum of the one-photon cross section for Xe [17].

All of these mechanisms rely on fine tuning the light frequency and require long, low-intensity pulses. In contrast, our mechanism does not rely on frequency tuning or intermediate resonances. It operates in the strong-field regime, for a broad range of frequencies and for short pulses. Spin polarization is achieved via spin-orbit interaction in the ionic core and is due to the interplay of (i) the electron-core entanglement and (ii) the sensitivity of ionization in circularly polarized fields to the sense of electron rotation in the initial state.

Consider strong-field ionization of noble gas atoms by right circularly polarized field propagating in the positive direction of the z axis. For all noble gas atoms except helium, the outer shell is filled by six p electrons. Thus, there is no spin-orbit interaction in the ground state and there is an equal amount of p_+ and p_- electrons, "counter-rotating" and "co-rotating" with the field. We have recently shown [18,19] that nonadiabatic effects in strong-field ionization result in its high sensitivity to the sense of electron rotation in the initial state: circularly polarized infrared laser field preferentially removes counter-rotating electrons. Our theoretical prediction regarding the sensitivity of strong field ionization to the sense of electron rotation in the initial state has now been confirmed [see Ref. [20] for detailed comparison of theory and experiment] by the experiment [21].

Electron removal leaves the p shell open. Spin-orbit interaction splits the states of the ion with respect to the total angular momentum of the core $J = 1/2$ and $J = 3/2$, providing two ionization channels with slightly different ionization potentials. Just like in the EPR experiment, once we divided the system with total angular momentum $J = 0$, $L = 0$, and $S = 0$ into two parts electron and the core, we know that $m_j = -M_J$, $m_s = -M_s$, where capital letters and small letters are for the initial values of the quantum numbers for the core and the electron, correspondingly.

Ionization of $m_l = 0$ is strongly suppressed. The right circular field preferentially removes the p^- electron [18,19], thus, $m_l = -1$. Suppose we have created the ion in the $^2P_{1/2}$ state: For the core $J = 1/2$, $|M_J| = 1/2$, $L = 1$ and therefore M_L and M_S have the opposite sign. Thus, the p^- electron correlated to the state $^2P_{1/2}$ must have had $|m_j| = 1/2$ and m_l opposite to m_s, yielding $m_s = 1/2$ for the initial value $m_l = -1$. Thus, the interplay of electron-ion entanglement and sensitivity of ionization to initial m_l lead to spin polarization. 100% selectivity of ionization to the sense of rotation of the electron in the ground state would lead to 100% spin polarization in the channel $^2P_{1/2}$. Spin polarization in the channel $^2P_{3/2}$ is less than 100%, since the total momentum of the core $J = 3/2$ admits both $|m_j| = 3/2$ and $|m_j| = 1/2$ of the correlated photoelectron. The ability to separate photoelectron spectra corresponding to $^2P_{3/2}$ and $^2P_{1/2}$ ionization channels experimentally [22,23] offers opportunities for achieving a high degree of spin polarization of coherent electron beams produced by strong-field ionization. Note that similar separation of strong-field photoelectron spectra correlated to different core states of a polyatomic molecule has recently been demonstrated in [24] and used to identify different channels in strong-field ionization.

To provide a quantitative picture of the effect, we extend our method [18,19] to include spin-orbit interaction. The extension is based on angular momentum algebra and does not contain any further approximations. Pertinent theoretical work in the case of linearly polarized fields includes Refs. [25,26].

Nonadiabatic ionization rates for atomic p_m orbitals ($m = 0,\pm1$) in left ($c = -1$) or right ($c = +1$) circularly polarized laser fields can be written as a sum over multiphoton channels [18,19],

$$w_c^{p_m}(\mathcal{E},\omega,I_p) = \sum_{n\geqslant n_0}^{\infty} w_{nc}^{p_m}(\mathcal{E},\omega,I_p), \tag{1}$$

where $n_0 = (2U_p + I_p)/\omega$. Summation leads to the following simple expression [18,19]:

$$w_c^{p_m}(\mathcal{E},\omega,I_p) = |C_{\kappa l=1}|^2 I_p \frac{\mathcal{E}}{2\mathcal{E}_0} h_c^{p_m}(\gamma) e^{-\frac{2\mathcal{E}_0}{3\mathcal{E}} g(\gamma)}. \tag{2}$$

In Eqs. (1) and (2), $\mathcal{E}$ is the electric field amplitude, ω is the laser frequency, I_p is the ionization potential, $U_p = \mathcal{E}^2/(4\omega^2)$ is the pondermotive potential, $\mathcal{E}_0 = (2I_p)^{3/2}$, $\gamma = \sqrt{2I_p}\,\omega/\mathcal{E}$ is the Keldysh parameter [27]. The coefficient $C_{\kappa l=1}$ characterizes the asymptotic behavior of the radial wave function, depending on $\kappa = \sqrt{2I_p}$ and the orbital quantum number l, with $l = 1$ for p_m orbitals. The exponential factor $g(\gamma)$ [18,19] does not depend on the sense of circular polarization $c = \pm1$ and on the parameters of atomic orbital. The orbital dependence comes from the prefactors $h_c^{p_0}(\gamma)$ and $h_c^{p_\pm}(\gamma)$ for p_0 and $p_\pm$ orbitals as shown in Refs. [18,19] and results in higher ionization rates for p_- orbitals than for p_+ orbitals in right circularly polarized laser fields ($c = +1$).

The relationship between the ionization rates from the nonrelativistic orbitals considered above and the relativistic spin orbitals p_{jm_j} with total (orbital and spin) angular quantum number j and a corresponding magnetic quantum number m_j obtains using angular momentum algebra. The spin-orbitals p_{jm_j} can be expanded in the basis of the products of orbitals p_m and spin functions χ_{sm_s} as

$$p_{jm_j} = \sum_{m,m_s} C^{jm_j}_{1m,\frac{1}{2}m_s} p_m \chi_{\frac{1}{2}m_s}, \tag{3}$$

where the expansion coefficients $C^{jm_j}_{lm,sm_s}$ are the Clebsch-Gordan coefficients with orbital and spin quantum numbers $l = 1$ and $s = 1/2$, respectively; the corresponding magnetic quantum numbers m and m_s are restricted by $m + m_s = m_j$. Integrating the corresponding density over the spin variable σ yields the orbital density of spin orbitals p_{jm_j},

$$\int |p_{jm_j}|^2 d\sigma = \sum_{m,m_s} \left|C^{jm_j}_{1m,\frac{1}{2}m_s}\right|^2 |p_m|^2. \tag{4}$$

The same relations hold for the momentum representation of spin orbitals $\tilde{p}_{jm_j}$, i.e.,

$$\int |\tilde{p}_{jm_j}|^2 d\sigma = \sum_{m,m_s} \left|C^{jm_j}_{1m,\frac{1}{2}m_s}\right|^2 |\tilde{p}_m|^2, \tag{5}$$

where $\tilde{p}_m$ is the momentum representation of orbitals p_m. Since the strong-field ionization rates [Eqs. (1) and (2)] depend linearly on $|\tilde{p}_m|^2$ (see Refs. [18,19]), we can express the ionization rate for the spin orbitals p_{jm_j} [Eq. (5)] via ionization rates for p_m orbitals: It yields the general formula for the ionization rates for p_{jm_j} spin orbitals,

$$w_c^{p_{jm_j}}\left(\mathcal{E},\omega,I_p^{P_j}\right) = \sum_{m,m_s} \left|C^{jm_j}_{1m,\frac{1}{2}m_s}\right|^2 w_c^{p_m}\left(\mathcal{E},\omega,I_p^{P_j}\right), \tag{6}$$

in particular

$$w_c^{p_{\frac{1}{2}\pm\frac{1}{2}}}\left(\mathcal{E},\omega,I_p^{P_{\frac{1}{2}}}\right) = \tfrac{2}{3} w_c^{p_\pm}\left(\mathcal{E},\omega,I_p^{P_{\frac{1}{2}}}\right) + \tfrac{1}{3} w_c^{p_0}\left(\mathcal{E},\omega,I_p^{P_{\frac{1}{2}}}\right), \tag{7}$$

$$w_c^{p_{\frac{3}{2}\pm\frac{1}{2}}}\left(\mathcal{E},\omega,I_p^{P_{\frac{3}{2}}}\right) = \tfrac{1}{3} w_c^{p_\pm}\left(\mathcal{E},\omega,I_p^{P_{\frac{3}{2}}}\right) + \tfrac{2}{3} w_c^{p_0}\left(\mathcal{E},\omega,I_p^{P_{\frac{3}{2}}}\right), \tag{8}$$

$$w_c^{p_{\frac{3}{2}\pm\frac{3}{2}}}\left(\mathcal{E},\omega,I_p^{P_{\frac{3}{2}}}\right) = w_c^{p_\pm}\left(\mathcal{E},\omega,I_p^{P_{\frac{3}{2}}}\right), \tag{9}$$

or as a sum over multiphoton channels,

$$w_c^{p_{jm_j}}\left(\mathcal{E},\omega,I_p^{P_j}\right) = \sum_{n\geqslant n_0}^{\infty} w_{nc}^{p_{jm_j}}\left(\mathcal{E},\omega,I_p^{P_j}\right), \tag{10}$$

where

$$w_{nc}^{p_{jm_j}}\left(\mathcal{E},\omega,I_p^{P_j}\right) = \sum_{m,m_s} \left|C^{jm_j}_{1m,\frac{1}{2}m_s}\right|^2 w_{nc}^{p_m}\left(\mathcal{E},\omega,I_p^{P_j}\right). \tag{11}$$

Here, $I_p^{P_J}$ is the J-dependent ionization potential due to spin-orbit splitting between $^2P_{1/2}$ and $^2P_{3/2}$ states of the ion. The quantum number $m_s = \pm1/2$ in Eqs. (6) and (11) indicate projection of the electron spin on the laser propagation direction. Thus, Eqs. (6) and (11) provide information on spin-resolved ionization rates. Total spin polarization is proportional to the difference in the total ionization rates for the photoelectrons with spin-up $w_{c\uparrow}(\mathcal{E},\omega)$ and spin-down $w_{c\downarrow}(\mathcal{E},\omega)$:

$$P_c(\mathcal{E},\omega) = \frac{w_{c\uparrow}(\mathcal{E},\omega) - w_{c\downarrow}(\mathcal{E},\omega)}{w_{c\uparrow}(\mathcal{E},\omega) + w_{c\downarrow}(\mathcal{E},\omega)}. \tag{12}$$

Using Eq. (6), total spin-resolved ionization rates can be expressed via m-resolved ionization rates $w_c^{p_m}$:

$$\begin{aligned} w_{c\uparrow,\downarrow}(\mathcal{E},\omega) = {} & \tfrac{1}{3} w_c^{p_0}\left(\mathcal{E},\omega,I_p^{P_{\frac{1}{2}}}\right) + \tfrac{2}{3} w_c^{p_0}\left(\mathcal{E},\omega,I_p^{P_{\frac{3}{2}}}\right) \\ & + w_c^{p_\pm}\left(\mathcal{E},\omega,I_p^{P_{\frac{3}{2}}}\right) + \tfrac{2}{3} w_c^{p_\mp}\left(\mathcal{E},\omega,I_p^{P_{\frac{1}{2}}}\right) \\ & + \tfrac{1}{3} w_c^{p_\mp}\left(\mathcal{E},\omega,I_p^{P_{\frac{3}{2}}}\right), \end{aligned} \tag{13}$$

where the upper superscript in $w_c^{p_\pm}$ should be used for spin-up ($\uparrow$) and the lower superscript should be used for spin-down ($\downarrow$) rates, correspondingly.

In particular, neglecting small contribution of $w_c^{p_0}$ [19] in Eq. (13), yields simple and accurate expressions for spin polarization of electron correlated to states $^2P_{1/2}$:

$$P_c\left(\mathcal{E},\omega,I_p^{P_{\frac{1}{2}}}\right) \simeq 2\,\mathrm{sgn}(c)\,\frac{A(\gamma)}{1+A(\gamma)^2}, \tag{14}$$

and $^2P_{3/2}$:

$$P_c\left(\mathcal{E},\omega,I_p^{P_{\frac{3}{2}}}\right) \simeq -\mathrm{sgn}(c)\,\frac{A(\gamma)}{1+A(\gamma)^2}, \tag{15}$$

where

$$A(\gamma) = \frac{\zeta_0}{\gamma}\sqrt{\frac{1+\gamma^2}{\zeta_0^2/\gamma^2+1}}. \tag{16}$$

Here γ is the Keldysh parameter and the parameter $0 \leqslant \zeta_0 \leqslant 1$ satisfies the equation $\sqrt{\frac{\zeta_0^2+\gamma^2}{1+\gamma^2}} = \tanh\frac{1}{1-\zeta_0}\sqrt{\frac{\zeta_0^2+\gamma^2}{1+\gamma^2}}$. Note that $\zeta_0 \simeq \gamma^2/3$ for $\gamma \ll 1$, and $\zeta_0 \simeq 1 - 1/\ln\gamma$ for $\gamma \gg 1$ [28].

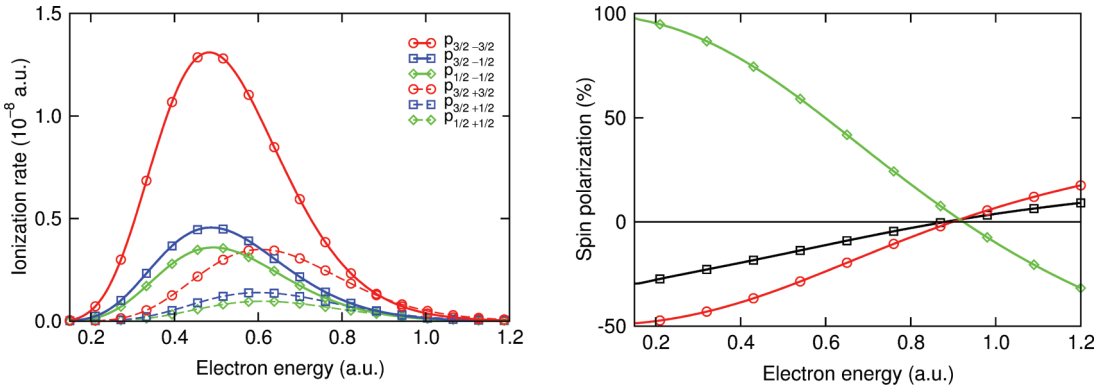

FIG. 1. (Color online) Left panel shows photoelectron energy distribution [Eq. (11)] for p_{jm_j} spin orbitals. Right panel shows spin polarization of photoelectrons [Eq. (17)] resolved on the $^2P_{1/2}$ state of the core (green curve with diamonds), $^2P_{3/2}$ state of the core (red curve with circles), and integrated over core states (black curve with squares), for krypton atom, ionization potentials $I_p^{P_{3/2}} = 0.5145$ a.u. and $I_p^{P_{1/2}} = 0.5389$ a.u., and right circularly polarized field with frequency $\omega = 0.057$ a.u. (800 nm) and field strength $\mathcal{E} = 0.05$ a.u. (1.8×10^{14} W/cm^2)

Effects of long-range potential equally affect the ionization rates $w_c^{p_\pm}$, $w_c^{p_0}$ [18,19] and thus they do not affect results for spin polarization given by Eqs. (14) and (15).

Prior to the analysis of total spin polarization, it is essential to consider spin polarization resolved on the final electron energy and the final state of the core. Note that the latter is easily accomplished by energy discrimination of the photoelectron spectra correlated to different core states as in Refs. [23,24]. It is obtained using Eq. (11):

$$P_{nc}\left(\mathcal{E},\omega,I_p^{P_J}\right) = \frac{w_{nc\uparrow}\left(\mathcal{E},\omega,I_p^{P_J}\right) - w_{nc\downarrow}\left(\mathcal{E},\omega,I_p^{P_J}\right)}{w_{nc\uparrow}\left(\mathcal{E},\omega,I_p^{P_J}\right) + w_{nc\downarrow}\left(\mathcal{E},\omega,I_p^{P_J}\right)}, \qquad (17)$$

where the corresponding rates $w_{nc\uparrow}(\mathcal{E},\omega,I_p^{P_J})$ and $w_{nc\downarrow}(\mathcal{E},\omega,I_p^{P_J})$ are resolved on the number of absorbed photons, i.e., on the final electron energy: $E_{\rm kin} = (n - n_0)\omega$ [18,19]. Energy and spin-resolved ionization rates $w_{nc\uparrow,\downarrow}(\mathcal{E},\omega,I_p^{P_J})$ are expressed via energy and m-resolved ionization rates $w_{nc}^{p_m}$ given by Eq. (1) in the same way as in Eq. (13).

Energy and core-state resolved photoelectron spectra for Kr atom are shown in Fig. 1(a) for $\omega = 0.057$ a.u. and $\mathcal{E} = 0.05$ a.u. corresponding to 800-nm light with intensity 1.8×10^{14} W/cm^2. Solid and dashed lines represent contributions of counter-rotating and co-rotating electrons, resolved on the core states. The signals coming from co-rotating and counter-rotating electrons are spectrally shifted, reflecting nonadiabatic nature of strong-field ionization [18,19] for these typical laser parameters. The counter-rotating electrons dominate the low-energy part of the spectrum, whereas the co-rotating electrons dominate the high energy part of the spectrum.

Consider first the electrons correlated to the $^2P_{1/2}$ state of the core [green curves with diamonds in Fig. 1(a)]. As discussed above, for the $^2P_{1/2}$ states, the sense of electron rotation uniquely maps into the spin state: The solid green curve with diamonds corresponds to the spin-up electrons, while the dashed green curve with diamonds corresponds to the spin-down electrons. The signal coming from the counter-rotating electron (solid green curve with diamonds) is much stronger than the signal from the co-rotating electron in the low-energy part of the spectrum, leading to high, close to 100% spin polarization [see Fig. 1(b), green curve with diamonds] in the low energy part of the spectrum. Since the photoelectron peak correlated to the $^2P_{1/2}$ state is lower in energy than the one for the $^2P_{3/2}$ state, separating lowest-energy electrons is an efficient method of obtaining 100% spin polarization in strong-field ionization.

Consider now electrons correlated to the core state $^2P_{3/2}$. Had one-to-one mapping between the sense of electron rotation and the orientation of its spin existed for this core state, the respective contribution of the spin-up electron would have been given solely by the red dashed curve with circles, of the spin-down electrons solely by the red solid curve with circles. Thus, the spin polarization would have been given by a curve similar to the green curve with diamonds in Fig. 1(b), only with the opposite sign.

However, for the core state $^2P_{3/2}$ the picture becomes more complex, because the total momentum $J = 3/2$ has more projections on the z axis: $|M_J| = 3/2$ and $|M_J| = 1/2$. Each sense of electron rotation in the initial state (m_l) can pair with both projections of the electron spin m_s. For example, the counter-rotating electron, which dominates the overall signal, can have not only spin-down component (red solid curve with circles), but also spin-up (blue solid curve with squares) component. Naturally, for the counter-rotating electron the spin-down component (solid red curve with circles) dominates the spin-up (blue solid curve with squares) component, since $J = 3/2$ has larger probability to have maximal possible value of the projection $|M_J| = 3/2$ (i.e., larger Clebsch-Gordan coefficient). For the same reason, the spin-up component of the co-rotating electron (red dashed curve with circles) dominates its spin-down component (blue dashed curve with squares). The interplay of these four spectra is responsible for decreased spin polarization for the electron correlated to the $^2P_{3/2}$ core state [compare Fig. 1(b), red curve with circles vs Fig. 1(b), green curve with diamonds].

Electrons correlated to different core states have spin polarization of opposite sign and therefore the total energy-resolved spin polarization, integrated over the two core states [Fig. 1(b), black curve with squares], is even lower.

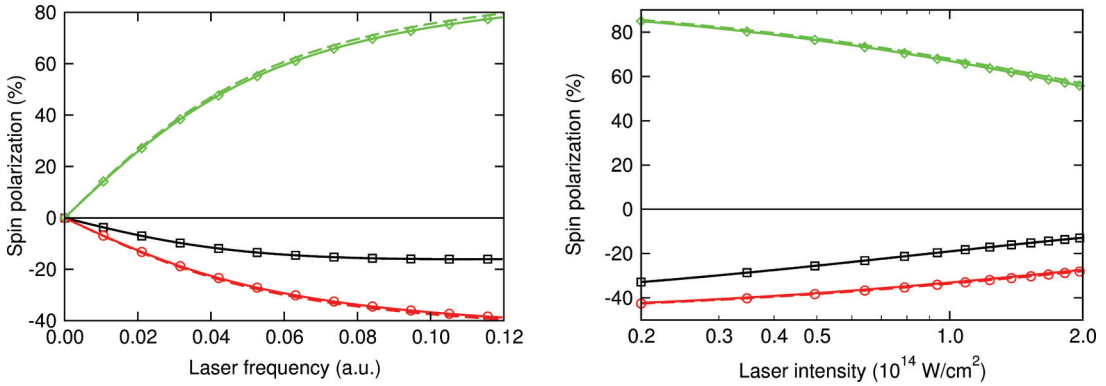

FIG. 2. (Color online) Control of spin polarization in strong field ionization of Kr (ionization potentials $I_p^{P_{3/2}} = 0.5145$ a.u. and $I_p^{P_{1/2}} = 0.5389$ a.u.) by right circularly polarized laser field. Energy-integrated spin polarization resolved on the $^2P_{1/2}$ state of the core [green curve with diamonds, accurate; corresponding dashed curve, approximate using Eq. (14)], $^2P_{3/2}$ state of the core [red curve with circles, accurate; corresponding dashed curve, approximate using Eq. (15)], and integrated over core states (black curve with squares). Left panel shows dependence on laser frequency, for the field strength $\mathcal{E} = 0.05$ a.u. Right panel shows dependence on the laser intensity, for the laser frequency $\omega = 0.057$ a.u. (800 nm).

Such integral energy-resolved spin polarization is particularly relevant when spectral peaks corresponding to different core states cannot be resolved, e.g., for short laser pulses.

Spin polarization in strong-field ionization is a manifestation of the nonadiabatic nature of the process. It vanishes in the limit of the small Keldysh parameter [27] γ, when ionization rates for co-rotating and counter-rotating electrons become equal [18,19]. Nonadiabaticity increases with increasing γ, offering opportunities for controlling spin polarization of electron beams. Figures 2(a) and 2(b) shows the degree of spin polarization integrated over the final electron energy and illustrates opportunities for its frequency and intensity control. The degree of spin polarization can be particularly well manipulated via frequency control.

Integrated spin polarization naturally depends on the strength of spin-orbit interaction. For example, for laser frequency $\omega = 0.057$ a.u. (800 nm), laser amplitude $\mathcal{E} = 0.03$ a.u., and right circular polarization, the degree of energy and core state integrated spin polarization is -23.4% for krypton, -31.1% for xenon, and -34.3% for radon. Note that, due to the exponential sensitivity of strong field ionization to the ionization potential, large spin-orbit splitting leads to the suppression of ionization in channel $^2P_{1/2}$. In this case, total spin polarization is given by Eq. (15) and can never exceed 50%.

Our work opens several new opportunities.

First, application of strong laser fields provides the opportunity to create short, dense spin-polarized electron and ion beams by using a few tens of femtoseconds pulses. Short electron pulses could be interesting for time-resolved electron diffraction experiments. Development of femtosecond electron diffraction with coherent, ultrashort, single electron wave packets is a new direction in ultrafast spectroscopy [2,30,31]. One of the options involves an optical pump-electron probe scheme. Near-IR and mid-IR laser pulses are used to generate single electron wave packets from nanosized particles: metallic tip or dielectrics such as, e.g., carbon or silicon nanoparticles. In the latter case, the strong field ionization is similar to isolated atoms [32]. Since both carbon and silicon have p electrons in the outer shell, our results show that spin-polarized electron pulses will be produced. Thus, femtosecond temporal resolution can be combined with spin polarization, adding additional capability to ultrafast coherent structural probes. Second, our analysis is not restricted to noble gas atoms. Similar effects should occur in linear and ring-shaped molecules with degenerate HOMO and ground singlet state. They should yield higher degree of total integrated spin polarization than atoms, because spin-orbit states in such molecules have lower degeneracy than in atoms. Twofold degeneracy [e.g., Eq. (14)] of the lowest ionic state will yield up to 100% of total spin polarization, whereas fourfold degeneracy of lowest ionic state [e.g., Eq. (15)] yields maximum 50% of total spin polarization. Third, relatively strong total spin polarization signal can be used to probe chiral molecules with strong fields, extending similar capabilities of the one-photon spin polarization spectroscopy [29].

We gratefully acknowledge stimulating discussions with Prof. M. Ivanov and Prof. R. Dörner. We are grateful to Prof. P. Lambropoulos for his insightful comments on spin-polarization in multiphoton regime. This work was supported by the DFG Grant No. Sm 292/2-1.

[1] F. Krausz and M. Ivanov, Rev. Mod. Phys. **81**, 163 (2009).
[2] M. Krüger, M. Schenk, M. Förster, and P. Hommelhoff, J. Phys. B **45**, 074006 (2012).
[3] P. Eckle *et al.*, Nat. Phys. **4**, 565 (2008).
[4] P. Eckle *et al.*, Science **322**, 1525 (2008).
[5] H. Akagi *et al.*, Science **325**, 1364 (2009).
[6] A. P. Pfeiffer *et al.*, Nat. Phys. **7**, 428 (2011).
[7] M. Meckel *et al.*, Science **320**, 1478 (2008).
[8] M. Spanner, O. Smirnova, P. B. Corkum, and M. Y. Ivanov, J. Phys. B **37**, L243 (2004).

[9] C. Blaga *et al.*, Nature (London) **483**, 194 (2012).
[10] Y. Huismans *et al.*, Science **331**, 61 (2011).
[11] U. Fano, Phys. Rev. **79**, 131 (1969).
[12] N. A. Cherepkov, J. Phys. B **14**, 2165 (1981).
[13] P. Lambropoulos, Phys. Rev. Lett. **30**, 413 (1973).
[14] P. Lambropoulos, J. Phys. B **7**, L33 (1974).
[15] S. N. Dixit, P. Lambropoulos, and P. Zoller, Phys. Rev. A **24**, 318 (1981).
[16] M. R. Teague and P. Lambropoulos, J. Phys. B **9**, 1251 (1976).
[17] T. Nakajima and P. Lambropoulos, Europhys. Lett. **57**, 25 (2002).
[18] I. Barth and O. Smirnova, Phys. Rev. A **84**, 063415 (2011); **85**, 029906(E) (2012); **85**, 039903(E) (2012).
[19] I. Barth and O. Smirnova, Phys. Rev. A **87**, 013433 (2013).
[20] I. Barth and O. Smirnova, Phys. Rev. A **87**, 065401 (2013).
[21] T. Herath, L. Yan, S. K. Lee, and W. Li, Phys. Rev. Lett. **109**, 043004 (2012).
[22] P. Agostini *et al.*, Phys. Rev. Lett. **42**, 1127 (1979).
[23] H. Rottke, J. Ludwig, and W. Sandner, J. Phys. B **29**, 1479 (1996).
[24] A. E. Boguslavskiy *et al.*, Science **335**, 1336 (2012).
[25] R. Santra, R. W. Dunford, and L. Young, Phys. Rev. A **74**, 043403 (2006).
[26] A. S. Kornev and B. A. Zon, Phys. Rev. A **85**, 035402 (2012).
[27] L. V. Keldysh, Sov. Phys. JETP **20**, 1307 (1965).
[28] A. M. Perelomov, V. S. Popov, and M. V. Terent'ev, Sov. Phys. JETP **23**, 924 (1966).
[29] U. Heinzmann and J. H. Dil, J. Phys.: Condens. Matter **24**, 173001 (2012).
[30] A. Paarmann *et al.*, J. Appl. Phys. **112**, 113109 (2012).
[31] G. Herink, D. R. Solli, M. Gulde, and C. Ropers, Nature (London) **483**, 190 (2012).
[32] S. Zherebtsov *et al.*, Nature Phys. **7**, 656 (2011).